ADVANCED FUNCTIONAL MATERIALS
www.afm-journal.de

Self-Powered Electronics by Integration of Flexible Solid-State Graphene-Based Supercapacitors with High Performance Perovskite Hybrid Solar Cells

Pengcheng Du, Xiaowen Hu, Chao Yi, Huckleberry C. Liu, Peng Liu, Hao-Li Zhang, and Xiong Gong**

To develop high-capacitance flexible solid-state supercapacitors and explore its application in self-powered electronics is one of ongoing research topics. In this study, self-stacked solvated graphene (SSG) films are reported that have been prepared by a facile vacuum filtration method as the free-standing electrode for flexible solid-state supercapacitors. The highly hydrated SSG films have low mass loading, high flexibility, and high electrical conductivity. The flexible solid-state supercapacitors based on SSG films exhibit excellent capacitive characteristics with a high gravimetric specific capacitance of 245 F g^{-1} and good cycling stability of 10 000 cycles. Furthermore, the flexible solid-state supercapacitors are integrated with high performance perovskite hybrid solar cells (pero-HSCs) to build self-powered electronics. It is found that the solid-state supercapacitors can be charged by pero-HSCs and discharged from 0.75 V. These results demonstrate that the self-powered electronics by integration of the flexible solid-state supercapacitors with pero-HSCs have great potential applications in storage of solar energy and in flexible electronics, such as portable and wearable personal devices.

1. Introduction

Recently, pervoskite hybrid solar cells (pero-HSCs) as an alternative to silicon-based photovoltaics have attracted significant attention due to their promising high power conversion efficiency (PCE).[1–3] The PCEs of pero-HSCs have skyrocketed to over 19%.[4] However, pero-HSCs, same as other photovoltaics, have to be applied in sunlight to generate electric energy and their PCEs are dependent on the time, location, and weather.[5] In order to alleviate these problems, pero-HSCs would be better to integrate with energy storage devices, such as supercapacitors, to build self-powered electronics, which can store the electric energy generated by pero-HSCs.[6] Moreover, these self-powered electronics have potential applications in flexible electronics, such as portable and wearable personal devices.[7–9]

The supercapacitors, also known as electrochemical capacitors, are widely recognized as a new generation of clean energy-storage devices, owing to its high power density, fast charge–discharge rate, long cycling life, and good operational safety.[10–13] As compared with the supercapacitors fabricated by liquid materials, the light-weight flexible supercapacitors fabricated by all solid-state materials possess the advantages in the applications for portable and wearable devices.[14–16] Numerous efforts have been devoted to develop flexible solid-state supercapacitors based on nanostructured carbon materials.[17–21] Among these nanostructured materials, graphene was stood out to be one of excellent materials due to its excellent electrical conductivity, mechanical flexibility, large surface area, and good chemical stability.[22–24] Flexible solid-state supercapacitors have been fabricated by using graphene films,[25,26] graphene hydrogels,[27,28] and graphene fibers[29] as the free-standing electrode. In order to fabricate graphene-based supercapacitors with high charge–discharge rate, graphene films with 3D structure by chemical vapor deposition (CVD),[30] facile vacuum filtration,[25,31] and hydrothermal method[32] have been developed to produce the graphene films with high surface area.[33] However, 3D graphene films produced by either CVD or hydrothermal method need to be further posttreated, which greatly restricts its applications in fabrication of the solid-state supercapacitors.[32,34]

In this study, we report the fabrication of flexible solid-state supercapacitors based on self-stacked solvated graphene (SSG) films prepared by facile vacuum filtration as the free-standing electrode. The flexible solid-state supercapacitors exhibit the capacitance of 245 F g^{-1} at the current density of 1 A g^{-1} and maintain 83% original capacitance retention after 10 000 charge–discharge cycles. We further integrate SSG-based flexible solid-state supercapacitors with high-performance pero-HSCs to build self-powered electronics. It was found that the flexible solid-state supercapacitors can be charged by pero-HSCs under the AM 1.5 white light illumination. These results demonstrate that the self-powered electronics have great potential

P. C. Du, Dr. X. Hu, C. Yi, H. C. Liu, Prof. X. Gong
College of Polymer Science and Polymer Engineering
The University of Akron
Akron, OH 44325, USA
E-mail: xgong@uakron.edu
P. C. Du, Prof. P. Liu, Prof. H.-L. Zhang
College of Chemistry and Chemical Engineering
Lanzhou University
Lanzhou 730000, P.R. China
E-mail: haoli.zhang@lzu.edu.cn

DOI: 10.1002/adfm.201500335

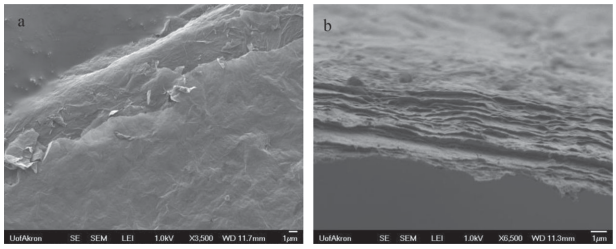

Figure 1. SEM images of the freeze-dried SSG films: a) surface SEM image and b) cross-section SEM image.

implications in the applications of storing solar energy and flexible electronics, such as portable and wearable personal devices.

2. Results and Discussion

As described in the Experimental Section, the free-standing SSG films were prepared by chemical converted graphene (CCG) dispersion through facile vacuum filtration.[25,31,35] **Figure 1**a presents the scanning electron microscopy (SEM) images of the freeze-dried SSG films. It is clear that the freeze-dried SSG films possess smooth surfaces; however, as shown in the cross-section image of the SSG films (Figure 1b), a uniform layer-by-layer structure is observed from entire SSG films. These results demonstrate that the SSG films formed a microporous structure between the graphene layers due to layer aggregation and π–π attractions within graphene.[26]

Figure 2a displays the Fourier transform IR (FT-IR) spectra of graphene oxide (GO) powder and CCG powder. The broad peak at 3400 cm^{-1} is attributed to the O–H group, the peak at 1740 cm^{-1} is assigned to the C=O stretching vibrations, and the peaks at 1365, 1425, and 1615 cm^{-1} are associated with the O–H deformations from the C–OH groups and water, respectively.[36,37] After GO was reduced by hydrazine hydrate in ammonia solution, the FT-IR spectrum was significantly changed. The intensity of asymmetric and symmetric C–O stretching from the C–O–C group became weak and the C=O peaked 1740 cm^{-1} is almost disappeared. These results indicate that the CCG was successfully prepared from GO.[38]

Raman spectroscopy was carried out to further confirm that the CCG was prepared from GO. As shown in Figure 2b, the GO powder, CCG powder, and the freeze-dried SSG films display both G band at ≈1582 cm^{-1} and D band at ≈1350 cm^{-1}.[36] However, the ratios of D/G for the CCG powder and the freeze-dried SSG films are higher than that of the GO powder, which is evidence that the GO powder was converted to the CCG powder.

By measuring the weight, it was found that the as-prepared SSG film contains about 94 wt% of water. After freeze-dried treatment, the thickness of the SSG film was decreased to 9 μm from 80 μm, which indicates that the as-prepared SSG film indeed has high hydrated hydrogel with high specific area than that of the freeze-dried graphene film. The electrical conductivities measured by four-probe method are ≈0.38 and ≈1.78 S cm^{-1} for the as-prepared SSG films and the freeze-dried SSG films, respectively. The electrical conductivity of the as-prepared SSG films is comparable to that of the dried graphene aerogels with 3D structure (≈0.87 S cm^{-1}).[39] These results indicate that the as-prepared SSG films possess high electrical conductivity.

Scheme 1 shows the detailed processing steps for fabrication of the flexible solid-state supercapacitors based on SSG films. **Figure 3**a,b present the capacitance behaviors of SSG films with a potential range from 0 to 1 V at various scan rates. As shown in Figure 3a, all cyclic voltammetry (CV) curves exhibit a nearly rectangular shape with no obvious peaks even at a high scan rate 500 mv s^{-1}, which indicate that the SSG films possess an ideal electrical double-layer capacitance.[40] The specific capacitance (C_s) of the solid-state supercapacitors can be calculated according to the equation of $C_s = 4(I\Delta t)/(m\Delta V)$, where I is the discharge current, Δt is the one cycle discharge time, m is the mass of the SSG film electrodes, and ΔV is the potential change after voltage drop during discharge, respectively. Figure 3c,d present the galvanostatic charge–discharge behaviors of the flexible solid-state supercapacitors based on SSG films. Based on the data presented in Figure 3c,d, the calculated C_s values at different current densities are shown in Figure 3e. The flexible solid-state supercapacitors based on as-prepared SSG films exhibit C_s of ≈250 F g^{-1} at the current density of 0.5 A g^{-1}. The C_s remains in 245 F g^{-1} at the current density of 1 A g^{-1}, which is 98% of its original values. Moreover, the solid-state supercapacitors still possess C_s of ≈145 F g^{-1}, which is 59% of its original value at the current density of 20 A g^{-1}. The decreased C_s at the high current densities is attributed to high internal resistance and slow ion diffusion rate in the solid electrolyte.[40] On the other hand, the flexible solid-state supercapacitors based on the freeze-dried SSG films only possess C_s of ≈181 F g^{-1} at the current density of 0.5 A g^{-1}. The C_s is decreased to ≈166 and ≈116 F g^{-1} at the current density of 1 and 20 A g^{-1}, respectively. The small C_s observed from the flexible solid-state supercapacitors base on the freeze-dried SSG films are likely due to the changes of porous structure and volume in the freeze-dried process, which hinders the infiltration of ions.[25]

In order to understand the underlying differences in the above two different supercapacitors, electrochemical impedance spectroscopy (EIS) measurement is carried out to investigate the electrical properties of the SSG

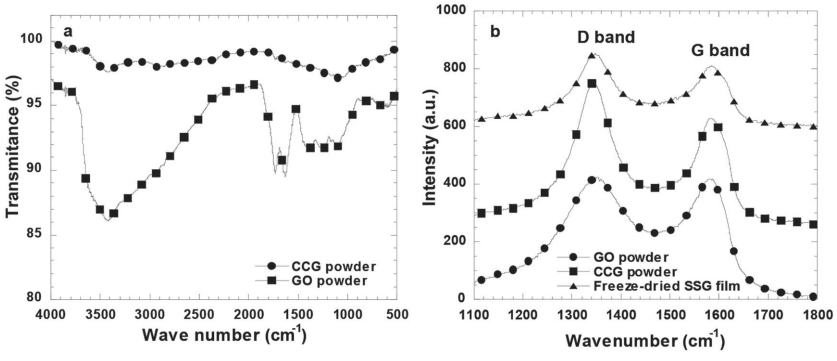

Figure 2. a) FT-IR spectra of GO and CCG powders and b) Raman spectra of GO powder, CCG powder, and the freeze-dried SSG films.

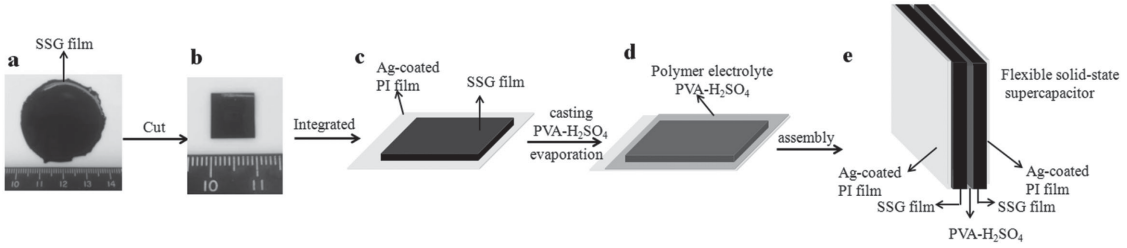

Scheme 1. Schematically diagram of fabrication of the flexible solid-state supercapacitors.

films. Figure 3f presents the Nyquist plots of the SSG films. The equivalent series resistances (R_S) defined by the high-frequency Nyquist plot, are 2.1 and 1.2 Ω for the as-prepared SSG films and the freeze-dried SSG films, respectively. These observations are in good agreement with the electrical conductivities measured by the four-probe method. The small R_s indicates the

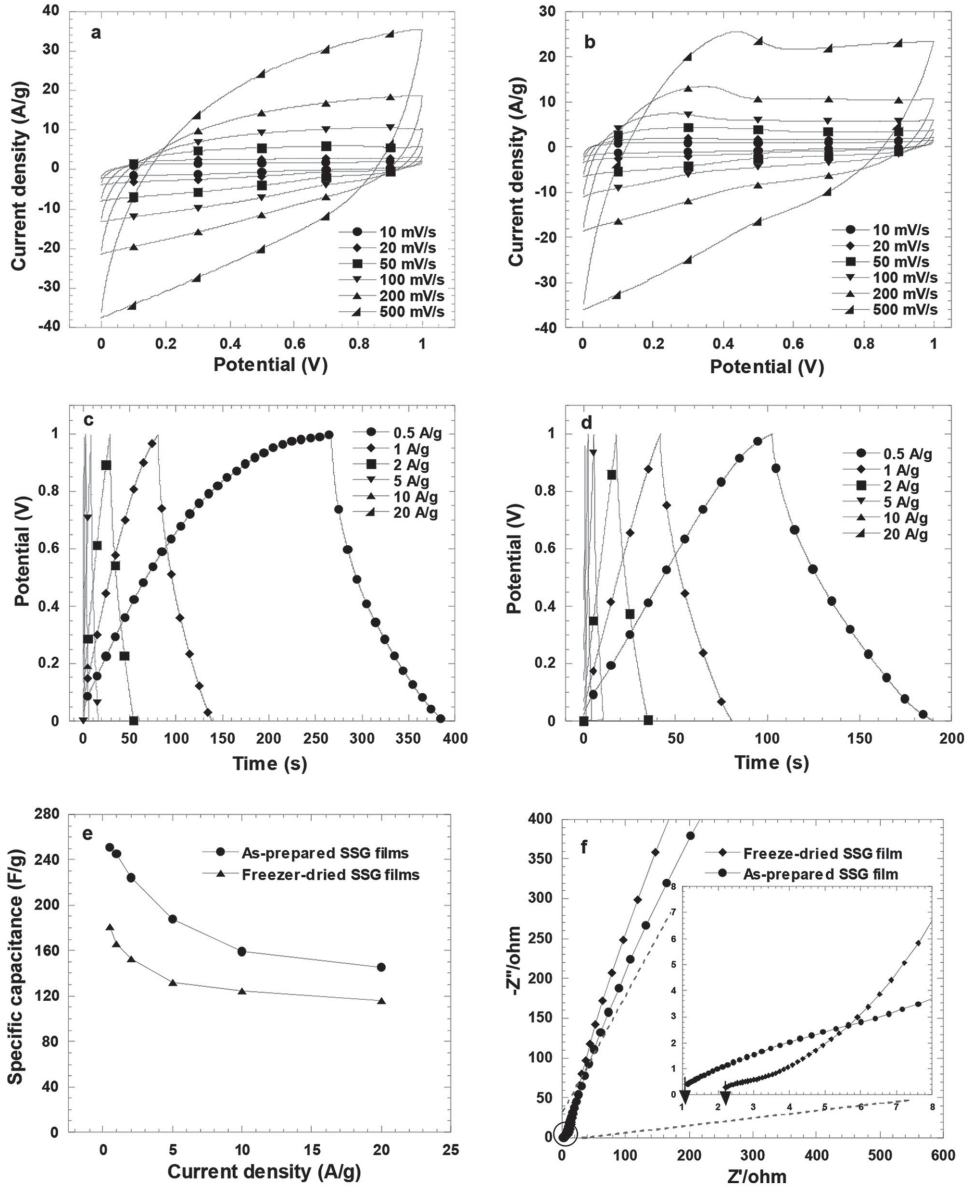

Figure 3. CV curves of solid-state supercapacitors based on a) the as-prepared SSG films and b) the freeze-dried SSG films; galvanostatic charge–discharge curves of solid-state supercapacitors based on c) the as-prepared SSG films and d) the freeze-dried SSG films; e) comparison of specific capacitances of the solid-state supercapacitors based on the as-prepared SSG films and the freeze-dried SSG films and f) Nyquist plots of the solid-state supercapacitors based on the as-prepared SSG films and the freeze-dried SSG films.

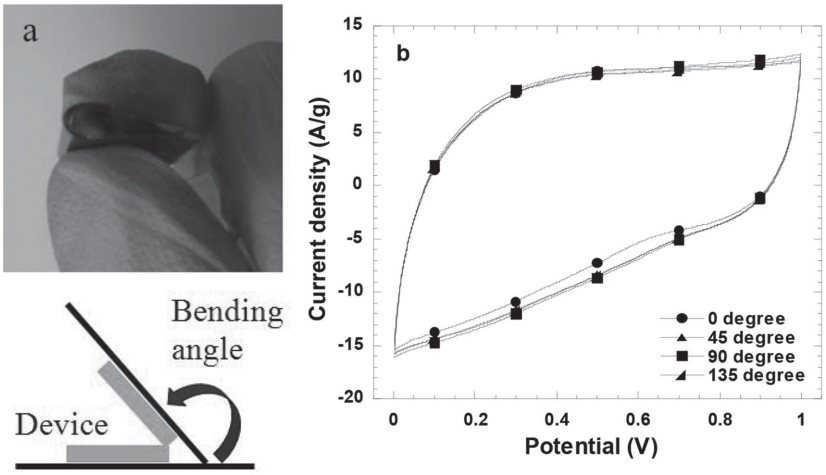

Figure 4. The mechanical properties of the flexible solid-state supercapacitors based on the as-prepared SSG films a) schematically show how the flexible solid-state supercapacitors was bend and b) CV curves of the flexible solid-state supercapacitors scan at 100 mV s^{-1} while the devices were bend at different bending angels.

supercapacitors possess small internal resistance.[38] The charge transfer resistance (R_{ct}) of the SSG films can be estimated from the diameter of the semicircle in the high frequency region. The small diameter of the semicircle indicates a small R_{ct}. It is obvious that the as-prepared SSG films possess smaller R_{ct} than that of the freeze-dried SSG films. The large R_{ct} from the freeze-dried SSG films was likely due to the changes of film morphology and the shrinkage of pore structures of the freeze-dried SSG films during the drying processes.[25,31]

The mechanical property of the flexible solid-state supercapacitors based on the as-prepared SSG films was further investigated. **Figure 4**a schematically displays how the flexible solid-state supercapacitors were bended. The CV curves of the solid-state supercapacitors bent at various angles are shown in Figure 4b. The flexible solid-state supercapacitors possess approximately the same capacitor behaviors and it is even bent at 135°, indicating that the solid-state supercapacitors have excellent mechanical properties.

The CV of the solid-state supercapacitors measured as it was prepared, stored for one-week and for one-month are shown in **Figure 5**a. It was found that there are improved capacitance for the supercapacitors stored after one-week and one-month. Such improvement is likely due to the ions that were further diffused inside of the SSG films. In order to further evaluate the cyclability and performance durability of the solid-state supercapacitors, the galvanostatic charge–discharge tests were carried out up to 10 000 cycles at the current density of 5 A g^{-1}. As shown in Figure 5b, the degradation of capacitance takes place mainly after 2000 cycles. The capacitance keeps 83% of its initial values after 10 000 cycles. These results demonstrate that the solid-state supercapacitors exhibit excellent stability and capacitive performance.

The energy density and the power density are two important parameters used to evaluate the performance of supercapacitors. The energy density (E) and the power density (P) can be calculated by $E = 1/2\ C_s \Delta V^2$ and $P = E/t$, respectively,[38,40] where C_s is the specific capacitance, ΔV is the potential change during the discharge process after voltage drop, and t is the discharge time of one cycle. **Figure 6** shows the correlation between E and P, which is termed as the Ragone plot. The flexible solid-state supercapacitors based on the as-prepared SSG films possess E of 8.01 Wh kg^{-1} at P of 5.97 kW kg^{-1}. The P can even reach to 10.1 kW kg^{-1} at E of 4.44 Wh kg^{-1}. However, the flexible solid-state supercapacitors based on the freeze-dried SSG films cannot possess such excellent energy density and power density. The E can only reach to 5.87 Wh kg^{-1} at P of 3.05 kW kg^{-1}, and the highest P reaches to 4.25 kW kg^{-1} at E of 4.31 Wh kg^{-1}. Both E and P from the solid-state supercapacitors based on the as-prepared SSG films are higher than those from the solid-state supercapacitors based on carbon nanotubes and other graphene films,[18,21,33,40–42] indicating that solid-state supercapacitors based on the as-prepared SSG films possess excellent performance of supercapacitors.

In order to explore the potential applications of the flexible solid-state supercapacitors based on the as-prepared SSG films, three supercapacitor units were connected in series to make a tandem supercapacitor. Each supercapacitor unit has the same area (1 × 1 cm^2) and same mass loading (≈0.4 mg for one electrode) of the SSG film. The CV and galvanostatic charge–discharge curves of both single supercapacitor and the tandem supercapacitors are shown in **Figure 7**a. It is clear that the potential windows are 1.0 and 3.0 V for single supercapacitor and tandem supercapacitors, respectively. The CV of the tandem supercapacitors almost expresses the rectangular structure. These observations were further confirmed by galvanostatic charge–discharge measurement, as shown in Figure 7b. The potential of the tandem supercapacitors can increase to 3 V, which is three times of that from single supercapacitor. Thus, these results indicate that the tandem supercapacitors have potentials to be used in some devices that need high voltage.

In order to explore potential application as new clean energy-storage devices,

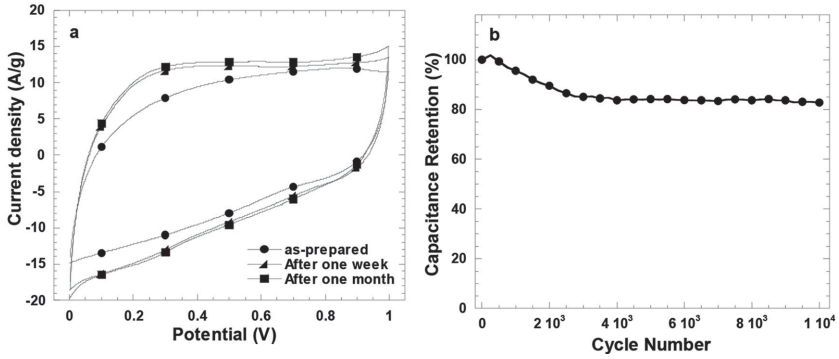

Figure 5. a) CV curves of the flexible solid-state supercapacitors stored at different time durations with scan rate at 100 mV s^{-1} and b) cycling stability of the flexible solid-state supercapacitors at the current density of 5 A g^{-1}.

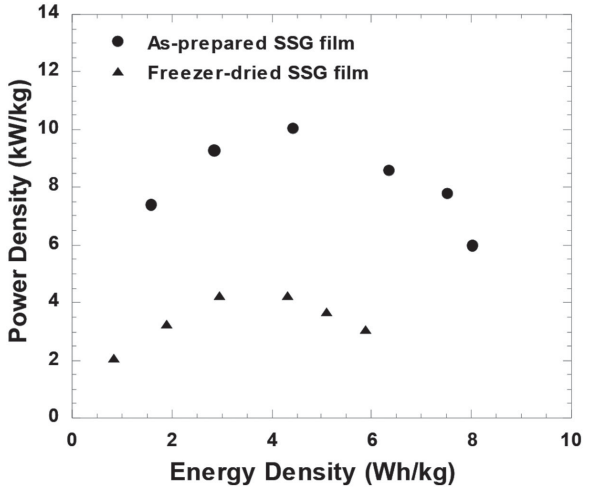

Figure 6. Ragone plots (power density vs energy density) of the flexible solid-state supercapacitors based on the as-prepared SSG films and the freeze-dried SSG films.

the solid-state supercapacitors is integrated with pero-HSCs. **Figure 8**a presents the *J–V* characteristics of pero-HSCs. The more details in pero-HSCs fabrication and characterization are reported in refs. [43–45]. The pero-HSCs exhibits a short-circuit current (J_{SC}) of 22.59 mA cm^{-2}, an open-circuit voltage (V_{OC}) of 0.90 V, a fill factor of 69.5%, with a corresponding PCE of 14.13%, which is comparable to that observed from the pero-HSCs fabricated by similar method and with the similar device structure.[1,2] The incident photon to current efficiency (IPCE) spectrum of pero-HSCs is presented in Figure 8b. The onset of the photocurrents observed from Figure 8b is at 800 nm, which is in good agreement with the bandgap of $CH_3NH_3PbI_{3-x}Cl_x$ observed from absorption spectrum.[46,47] Based on IPCE spectrum, the J_{SC} of pero-HSCs is estimated to be 21.14 mA cm^{-2}, which is consistent with that observed from the *J–V* characteristics (Figure 8a). It was reported that the photocurrent hysteresis are originated from the presence of traps, ferroelectrically respond in the perovskite materials and the ion migration in the perovskite films and interlayers, but the devices with negligible photocurrent hysteresis have also been reported in the case of perovskite/fullerene planar heterojunction solar cells provided that optimized perovskite films.[48–51] The photocurrent hysteresis of pero-HSCs is tested by sweeping the *J–V* measurement from both forward and reversed directions. The results are shown in Figure 8c. The efficiency difference between *J–V* under forward and reversed directions is less than 2%, which is probably attributed to high quality of perovskite film with high surface coverage. These results demonstrate that pero-HSCs possess high performance.

Figure 9a displays the schematic diagram of integration of the flexible solid-state supercapacitors with pero-HSCs. After integration of pero-HSCs with the solid-state supercapacitors to assemble the self-powered electronics, the solid-state supercapacitors are charged by pero-HSCs under the white light illumination. As shown in Figure 9b, the charged supercapacitors can discharge from 0.75 V, which is smaller than V_{OC} (0.90 V) of pero-HSCs, to 0 V at the current density 1 A g^{-1}, and can hold about 45 s discharge time as well. These results demonstrate that self-powered electronics by integration of the flexible solid-state supercapacitors with high performance pero-HSCs can store the solar energy from pero-HSCs and has potential implications in flexible electronics, such as portable and wearable personal devices.[52]

3. Conclusions

In summary, the SSG films prepared by a facile filtration method were used as the free-standing electrode in the flexible solid-state supercapacitors. The flexible solid-state supercapacitors exhibit a high specific capacitance of 245 F g^{-1} at 1 A g^{-1} and retain 83% of its original values up to 10 000 charge–discharge cycles. We further integrated the flexible solid-state supercapacitors with high performance pero-HSCs to build self-powered electronics. It was found that the solid-state supercapacitors can be charged by pero-HSCs and discharged from 0.75 V which is smaller than the open-circuit voltage of pero-HSCs. These results demonstrate that the self-powered electronics by integration of the flexible solid-state supercapacitors with pero-HSCs have great potential implications in the applications of storing solar energy and flexible electronics, such as portable and wearable personal devices.

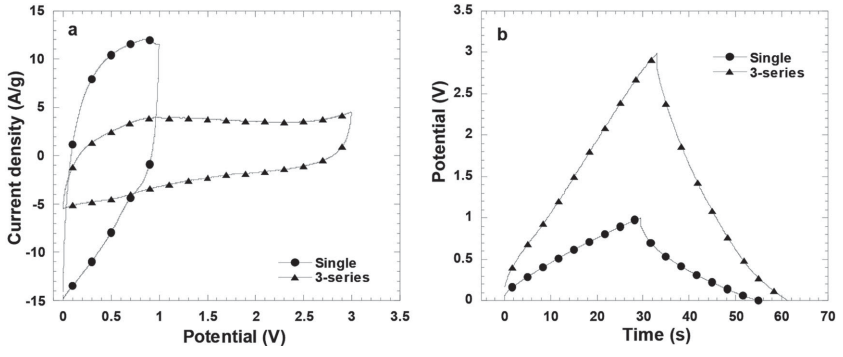

Figure 7. a) CV curves with scan rate at 100 mV s^{-1} and b) galvanostatic charge–discharge curves at 1 mA of a single solid-state supercapacitor and three solid-state supercapacitors in series.

4. Experimental Section

Materials: Graphite powder, hydrazine hydrate, poly(vinyl alcohol) (PVA) (molecular weight: 89 000–98 000 g mol^{-1}), ammonia methylamine solution (33 wt% in ethanol), hydriodic acid (57 wt% in water), and lead chloride ($PbCl_2$) were purchased from Sigma-Aldrich, used as received without further treatment. Poly(3,4-ethylenedioxythiophene):poly(styrenesulfonate) (PEDOT:PSS) and $PC_{61}BM$ were purchased from Clevious and 1-Material Inc., respectively. Methylammonium iodide (CH_3NH_3I) was synthesized according to reported reference.[2,3] To prepare the perovskite precursor solution, CH_3NH_3I and $PbCl_2$ powder were mixed in anhydrous dimethylformamide (Aldrich) with a molar ratio of 3:1. Specifically,

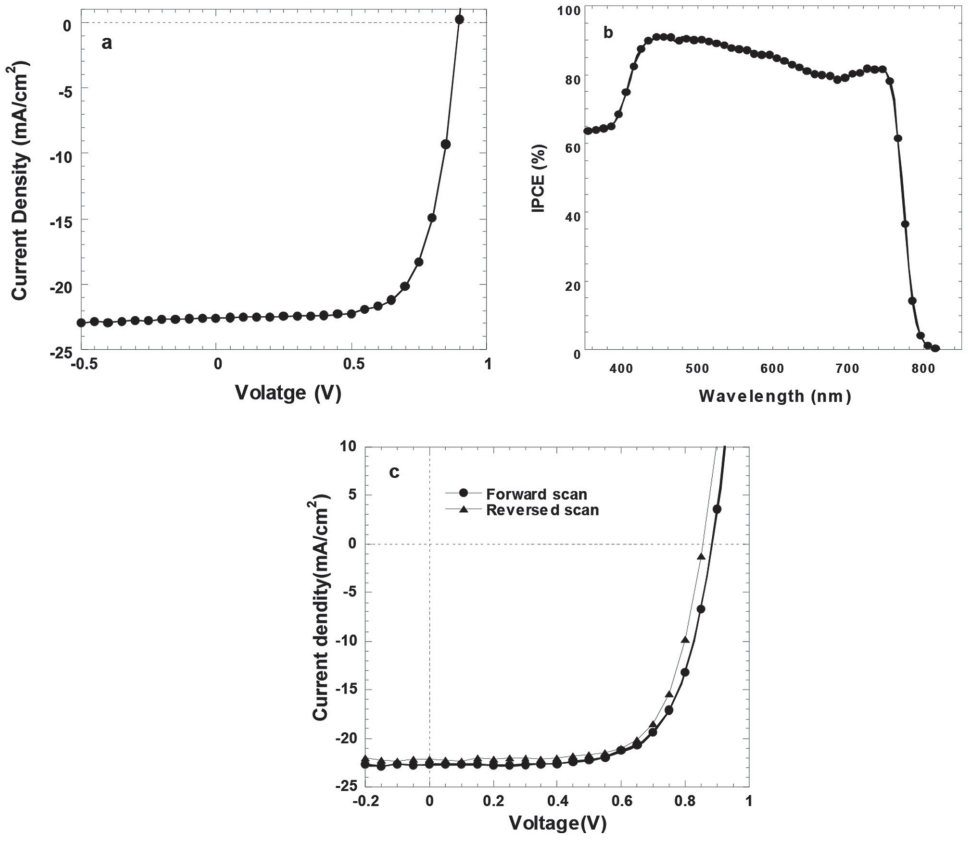

Figure 8. a) Current density–voltage characteristics of b) the IPCE spectrum of the pero-HSCs and c) photocurrents of pero-HSCs measured under forward and reversed directions.

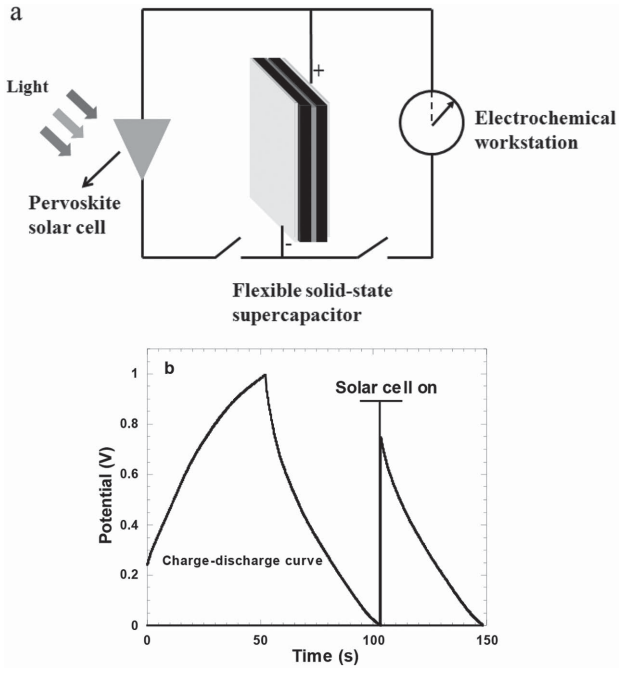

Figure 9. a) Schematically diagram of the integration of solid-state supercapacitors with perovskite solar cells and b) discharge curve of the flexible solid-state supercapacitors at the current density of 1 A g^{-1} after it was charged by perovskite solar cells.

the concentration of CH_3NH_3I and $PbCl_2$ were 2.64 and 0.88 M L^{-1}. The solution was stirred at 60 °C for 6 h and then placed for standstill overnight before device fabrication.

Preparation of SSG Films: GO was synthesized by oxidation of natural flake graphite following the modified Hummers' method.[35] A stable CCG dispersions was prepared by reducing the GO solution with hydrazine hydrated under ammonia aqueous. Then, SSG films were formed by using CCG dispersion through facile vacuum filtration.[21,31]

Characterization of SSG Films: SEM (S-2150 microscope, Hitachi, Japan) was carried out to investigate the film morphology of the freeze-dried SSG. The four-point method was used to measure the electrical conductivities of SSG films. Thermo Scientific DXR Raman Microscope using a 532 nm laser source and FT-IR Spectroscopy (Bruker Inc) were used to characterize the samples.

Fabrication of Flexible Solid-State Supercapacitors: The fabrication procedures for the flexible solid-state supercapacitors based on SSG films are schematically displayed in Scheme 1. The H_2SO_4-PVA gel electrolyte was prepared by first diluting 6 g H_2SO_4 (98%) into 30 mL deionized (DI) water and then adding the above H_2SO_4 solution into 6 g PVA with 30 mL DI water. The suspension solution was stirred at 85 °C until the solution became clear. After that the SSG film with thickness of ≈80 µm (step a) was cut into rectangular strips with an area of 1 cm × 1 cm and then dried the SSG film to the weight of ≈0.4 mg cm^{-2}, After that, the SSG film was immersed into 1 M H_2SO_4 solution overnight to allow H^+ protons to be infiltrated inside of the SSG film (step b). The SSG film was carefully assembled on the silver-coated polyimide substrate as one electrode (step c). After that, the H_2SO_4–PVA gel is casted on the top of SSG film from H_2SO_4–PVA water solution and then evaporated the excess water at room temperature for 12 h in the ambient condition to form the SSG film electrode coated with H_2SO_4–PVA solid-state electrolyte (step d). Finally, two SSG film electrodes coated with H_2SO_4–PVA solid-state electrolyte were face-to-face assembled together.

In this supercapacitor, the SSG film acts as the electrode, the H_2SO_4–PVA gel acts as the electrolyte and the separator as well (step e).

Characterization of Flexible Solid-State Supercapacitors: CV and galvanostatic charge–discharge measurement were conducted by using Gamry reference 3000 at the potential ranging from 0 to 1 V. EIS was measured in the frequency ranging from 10^5 to 10^{-2} Hz.

Fabrication of the Perovskite Hybrid Solar Cells (Pero-HSCs): The pero-HSCs were fabricated in the device with a configuration of ITO/PEDOT:PSS/$CH_3NH_3PbI_{3-x}Cl_x$/$PC_{61}BM$/Al, where ITO is indium tin oxide, $CH_3NH_3PbI_{3-x}Cl_x$ is perovskite materials, and Al is Aluminum. Approximately 35 nm of PEDOT:PSS was spin-coated on precleaned ITO glass substrates followed by thermal annealing at 150 °C for 10 min. The perovskite films were spin-coated on top of ITO/PEDOT:PSS from perovskite precursor solution in the glove box with nitrogen atmosphere. The perovskite thin films were processed by two-step procedures. In the first procedure, the spin-time was kept at 20 s, with the rotating-speed of 2500 rpm, but the acceleration-time was 10 s with the rotating-peed increased from 0 to 2500 rpm in the acceleration-time. In the second procedure, the acceleration-time was kept at 8 s, but the spin-time was tuned from 20 s, with the rotating-speed of 2500 rpm. The wet perovskite thin films were placed in petri-dish without cover for 30 min and then annealed at 90 °C for 3 h. Next, ≈100 nm of $PC_{61}BM$ was spin-coated on the top of perovskite thin films. Finally, ≈120 nm Al electrode was evaporated under high vacuum (2×10^6 mbar) through a shade mask. The device area is defined as 4.5 mm^2.

Characterization of Pero-HSCs: The current densities versus voltage (*J*–*V*) characteristics of pero-HSCs were recorded using a Keithley 2400 Source Meter. The device photocurrent was measured under air mass (AM) 1.5 illumination at the light intensity of 100 mW cm^{-2}. The light intensity was accurately calibrated by a standard Si photodiode. The Incident photon-to-current efficiency (IPCE) spectra of pero-HSCs were measured through the IPCE measurement setup in use at European solar test installation (ESTI) for cells and mini-modules. A 300 W steady-state xenon lamp provides the source light. Up to 64 filters (8–20 nm width, range from 300 to 1200 nm) are available on four filter-wheels to produce the monochromatic input, which is chopped at 75 Hz, superimposed on the bias light and measured via the usual lock-in technique.

Fabrication and Characterization of Self-Powered Electronics: The self-powered electronics were built by integration of the flexible solid-state supercapacitors with pero-HSCs through two-copper wires. The flexible solid-state supercapacitors were charged by the current generated from pero-HSCs under white light illumination. After the flexible solid-state supercapacitors were charged, the electrochemical workstation was connected with the copper wires to study the discharge properties of the flexible solid-state supercapacitors.

Acknowledgements

The authors would like to thank National Science Foundation Grant No. 1351785. P. C. Du and X. W. Hu would like to acknowledge the China Scholarship Council for the Joint Ph.D. program.

Received: January 26, 2015
Revised: February 11, 2015
Published online: March 21, 2015

[1] J. Burschka, N. Pellet, S. J. Moon, R. Humphry-Baker, P. Gao, M. K. Nazeeruddin, M. Grätzel, *Nature* **2013**, *499*, 316.
[2] O. Malinkiewicz, A. Yella, Y. H. Lee, G. M. Espallargas, M. Graetzel, M. K. Nazeeruddin, H. J. Bolink, *Nat. Photonics* **2014**, *8*, 128.
[3] K. G. Lim, H. B. Kim, J. Jeong, H. Kim, J. Y. Kim, T. W. Lee, *Adv. Mater.* **2014**, *26*, 6461.
[4] H. P. Zhou, Q. Chen, G. Li, S. Luo, T. B. Song, H. S. Duan, Z. R. Hong, J. B. You, Y. S. Liu, Y. Yang, *Science* **2014**, *345*, 542.
[5] P. H. Yang, X. Xiao, Y. Z. Li, Y Ding, P. F. Qiang, X. H. Tan, W. J. Mai, Z. Y. Lin, W. Z. Wu, T. Q. Li, H. Y. Jin, P. Y. Liu, J. Zhou, C. P. Wong, Z. L. Wang, *ACS Nano* **2013**, *7*, 2617.
[6] T. Chen, L. M. Dai, *J. Mater. Chem. A* **2014**, *2*, 10756.
[7] H. Nishide, K. Oyaizu, *Science* **2008**, *319*, 737.
[8] M. S. Whittingham, *MRS Bull.* **2008**, *33*, 411.
[9] K. Jost, D. Stenger, C. R. Perez, J. K. McDonough, K. Lian, Y Gogotsi, G. Dion, *Energy Environ. Sci.* **2011**, *4*, 3193.
[10] P. Aimon, Y. Gogotsi, *Nat. Mater.* **2008**, *7*, 845.
[11] G. P. Wang, L. Zhang, J. J. Zhang, *Chem. Soc. Rev.* **2012**, *41*, 792.
[12] T. Chen, L. M. Dai, *Mater. Today* **2013**, *16*, 272.
[13] Y. Gogotsi, P. Simon, *Science* **2011**, *334*, 917.
[14] C. Z. Meng, C. H. Liu, L. Z. Chen, C. H. Hu, S. S. Fan, *Nano Lett.* **2010**, *10*, 4025.
[15] Y. X. Xu, Z. Y. Lin, X. Q. Huang, Y. Wang, Y. Huang, X. F. Duan, *Adv. Mater.* **2013**, *25*, 5779.
[16] X. H. Lu, M. H. Yu, G. M. Wang, Y. X. Tong, Y. Li, *Energy Environ. Sci.* **2014**, *7*, 2160.
[17] D. Pech, M. Brunet, H. Durou, P. H. Huang, V. Mochalin, Y. Gogotsi, P. L. Taberna, P. Simon, *Nat. Nanotechnol.* **2010**, *5*, 651.
[18] T. Chen, H. S. Peng, M. Durstock, L. M. Dai, *Sci. Rep.* **2013**, *4*, 3612.
[19] Z. Q. Niu, J. Chen, H. H. Hng, J. Ma, X. D. Chen, *Adv. Mater.* **2012**, *24*, 4144.
[20] W. Wang, S. R. Guo, M. Penchev, I. Ruiz, K. N. Bozhilov, D. Yan, M. Ozkan, C. S. Ozkan, *Nano Energy* **2013**, *2*, 294.
[21] Z. Weng, Y. Su, D. W. Wang, F. Du, H. M. Cheng, *Adv. Energy Mater.* **2011**, *1*, 917.
[22] X. H. Cao, Z. Y. Yin, H. Zhang, *Energy Environ. Sci.* **2014**, *7*, 1850.
[23] Y. Huang, J. J. Liang, Y. S. Chen, *Small* **2012**, *8*, 1805.
[24] Y. W. Zhu, S. Murali, W. W. Cai, X. S. Li, J. W. Suk, J. R. Potts, R. S. Ruoff, *Adv. Mater.* **2010**, *22*, 3906.
[25] X. W. Yang, J. W. Zhu, L. Qiu, D. Li, *Adv. Mater.* **2011**, *23*, 2833.
[26] B. G. Choi, S. J. Chang, H. W. Kang, C. P. Park, H. J. Kim, W. H. Hong, S. G. Lee, Y. S. Huh, *Nanoscale* **2012**, *4*, 4983.
[27] H. C. Bi, K. B. Yin, X. Xie, Y. L. Zhou, N. Wan, F. Xu, F. Banhart, L. T. Sun, R. S. Ruoff, *Adv. Mater.* **2012**, *24*, 5124.
[28] Z. S. Wu, A. Winter, L. Chen, Y Sun, A. Turchanin, X. L. Feng, K. Müllen, *Adv. Mater.* **2012**, *24*, 5130.
[29] Z. L. Dong, C. C. Jiang, H. H. Cheng, Y. Zhao, G. Q. Shi, L. Jiang, L. T. Qu, *Adv. Mater.* **2012**, *24*, 1856.
[30] Z. Chen, W. Ren, L. Gao, B. Liu, S. Pei, H. Cheng, *Nat. Mater.* **2011**, *10*, 424.
[31] X. W. Yang, C. Cheng, Y. F. Wang, L. Qiu, D. Li, *Science* **2013**, *341*, 534.
[32] Y. Tao, X. Y. Xie, W. Lv, D. M. Tang, D. B. Kong, Z. H. Huang, H. Nishihara, T. Ishii, B. H. Li, D. Golberg, F. Y. Kang, T. Kyotani, Q. H. Yang, *Sci. Rep.* **2013**, *3*, 2975.
[33] C. H. Xu, B. H. Xu, Y. Gu, Z. G. Xiong, J. Sun, X. S. Zhao, *Energy Environ. Sci.* **2013**, *6*, 1388.
[34] S. Nardecchia, D. Carriazo, M. L. Ferrer, M. C. Gutierrez, F. del Monte, *Chem. Soc. Rev.* **2013**, *42*, 794.
[35] W. S. Hummers, R. E. Offerman, *J. Am. Chem. Soc.* **1958**, *80*, 1339.
[36] Y. X. Xu, H. Bai, G. W. Lu, C. Li, G. Q. Shi, *J. Am. Chem. Soc.* **2008**, *130*, 5856.
[37] N. I. Kovtyukhova, P. J. Ollivier, B. R. Martin, T. E. Mallouk, S. A. Chizhik, E. V. Buzaneva, A. D. Gorchinskiy, *Chem. Mater.* **1999**, *11*, 771.
[38] H. P. Cong, X. C. Ren, P. Wang, S. H. Yu, *Energy Environ. Sci.* **2013**, *6*, 1185.

[39] M. A. Worsley, P. J. Pauzauskie, T. Y. Olson, J. Biener, J. H. Satcher, T. F. Baumann, *J. Am. Chem. Soc.* **2010**, *132*, 14067.
[40] Y. X. Xu, Z. Y. Lin, X. Q. Huang, Y. Liu, Y. Huang, X. F. Duan, *ACS nano* **2013**, *7*, 4042.
[41] B. G. Choi, J. Hong, W. H. Hong, P. T. Hammond, H. Park, *ACS Nano* **2011**, *5*, 7205.
[42] Y. J. Kang, H. Chung, C. H. Han, W. Kim, *Nanotechnology* **2012**, *23*, 065401.
[43] K. Wang, C. Liu, P. C. Du, J. Zheng, X. Gong, *Energy Environ. Sci.* **2015**, DOI: 10.1039/c5ee00222b.
[44] K. Wang, C. Liu, P. C. Du, H. L. Zhang, X. Gong, *Small* **2015**, DOI 10.1002/smll.201403399.
[45] C. Liu, K. Wang, P. C. Du, T. Y. Yu, X. F. Yu, S. Cheng, X. Gong, *ACS Appl. Mater. Interfaces* **2015**, *7*, 1153.
[46] P. W. Liang, C. Y. Liao, C. C. Chueh, F. Zuo, S. T. Williams, X. K. Xin, J. J. Lin, A. K.-Y. Jen, *Adv. Mater.* **2014**, *26*, 3748.
[47] J. B. You, Z. R. Hong, Y. Yang, Q. Chen, M. Cai, T. B. Song, C. C. Chen, S. R. Lu, Y. S. Liu, H. P. Zhou, Y. Yang, *ACS Nano* **2014**, *8*, 1674.
[48] H. J. Snaith, A. Abate, J. M. Ball, G. E. Eperon, T. Leijtens, N. K. Noel, S. D. Stranks, J. T.-W. Wang, K. Wojciechowski, W. Zhang, *J. Phys. Chem. Lett.* **2014**, *5*, 1511.
[49] E. L. Unger, E. T. Hoke, C. D. Bailie, W. H. Nguyen, A. R. Bowring, T. Heumuller, M. G. Christoforo, M. D. McGehee, *Energy Environ. Sci.* **2014**, *7*, 3690.
[50] Q. Wang, Y. Shao, Q. Dong, Z. Xiao, Y. Yuan, J. Huang, *Energy Environ. Sci.* **2014**, *7*, 2359.
[51] J. W. Seo, S. Park, Y. C. Kim, N. J. Jeon, J. H. Noh, S. C. Yoonand, S. I. Seok, *Energy Environ. Sci.* **2014**, *7*, 2642.
[52] Z. T. Zhang, X. L. Chen, P. N. Chen, G. Z. Guan, L. B. Qiu, H. J. Lin, Z. B. Yang, W. Y. Bai, Y. F. Luo, H. S. Peng, *Adv. Mater.* **2014**, *26*, 466.